Compaction of granular materials: experiments and contact dynamics simulations

2006 J. Phys.: Conf. Ser. 40 133

(http://iopscience.iop.org/1742-6596/40/1/017)

Institute of Physics Publishing Journal of Physics: Conference Series **40** (2006) 133–143
doi:10.1088/1742-6596/40/1/017 Statistical Physics of Ageing Phenomena and the Glass Transition

Compaction of granular materials : experiments and contact dynamics simulations

G. Lumay, F. Ludewig and N. Vandewalle

GRASP, Institut de Physique B5, Université de Liège,
B-4000 Liège, Belgium.

E-mail: geoffroy.lumay@ulg.ac.be

Abstract.

We present an original experimental study of the slow compaction dynamics for two-dimensional isotropic granular systems. Compaction dynamics is measured at three different scales : the macroscopic scale through the normalized packing fraction $\tilde{\rho}$, the mesoscopic scale through the normalized fraction $\tilde{\phi}$ of domains ideally ordered in the system, and the microscopic scale through the grain mobility μ. The domains ideally ordered are found to obey a growth process dominated by the displacement of domain boundaries. We present also preliminary results of three-dimensional simulations with a model of contact dynamics. These results allow to discuss the difference between the two-dimensional and the three-dimensional cases.

1. Introduction

Granular matter has been the subject of numerous studies since the last decade [1, 2, 3, 4, 5]. Most of the industrial products are processed, transported and stocked in a granular state. The packing density of those granular materials becomes therefore a relevant parameter for a broad range of applications. The best way to reduce the costs for the manipulation of such granular materials is to increase the packing density ρ. This can be achieved by tapping or vibrating the vessel containing the grains.

Various experimental studies [6, 7, 9, 8, 10] have underlined the fact that the dynamics of compaction is a complex problem. The compaction is actually characterized by an extremely slow dynamics often compared with glassy dynamics or ageing. Different laws have been proposed for the increasing packing fraction ρ of a granular material with the number n of taps.

It has been proposed by Knight *et al.* [7], that the packing fraction obeys an inverse logarithmic law

$$\rho(n) = \rho_\infty - \frac{\rho_0 - \rho_\infty}{1 + B\ln(1 + \frac{n}{\tau})}, \tag{1}$$

where B and τ are dimensionless parameters. Both parameters ρ_0 and ρ_∞ are respectively the initial and the asymptotical packing fractions. This inverse logarithmic law was obtained in numerical models like the Tetris one [11, 12]and could also be derived from some theoretical arguments [13].

Some theoretical models [14, 15, 16] are based on a relationship between the mobility μ of the grains and the global density ρ of the packing. The mobility is a local property of the grains and corresponds to the grain ability to move inside the packing. By considering that the variation

of the density induced by a tap is proportional to the grain mobility, one can write the simple equation

$$\frac{\partial \rho}{\partial t} = k\ \mu, \tag{2}$$

where k is a constant. By considering a caging effect of the grains, some authors [14] proposed that the Vogel-Fulcher law for the decrease of the mobility μ with the density ρ. One has

$$\mu = \mu_0 \exp\left(-\frac{c}{1-\rho}\right). \tag{3}$$

This relation could be combined with Eq. (2) in order to obtain an inverse logarithmic behavior for $\rho(n)$. We can note that with colloidal systems, an increase in the volume fraction has been accurately related to a slowing down in the dynamics [17].

The slow dynamics of granular compaction has also been described by a cluster model [18]. A cluster is a group of grains ideally packed. The granular material is then considered as a system of various clusters competing in a random environment. Vibrations cause the slow growth of the cluster size. This growth leads to a logarithmic law for the evolution of the density. The relevant parameter for measuring any grain ordering is the fraction ϕ of grains ideally packed.

More recently, Philippe and Bideau [9] found that the compaction is better fitted by a stretched exponential

$$\rho(n) = \rho_\infty - (\rho_\infty - \rho_0) \exp\left[-\left(\frac{n}{\tau}\right)^\beta\right]. \tag{4}$$

This exponential law presents the great advantage to fit a saturation of the density which is sometimes accessible in experiments (for larges n values). Both parameters τ and β correspond respectively to a characteristic tap number and the stretching exponent. One should notice that in the experiments of Philippe and Bideau, the steady state corresponds to a dynamical balance between convection and compaction.

In this proceeding, we present an experimental study of compaction for spherical particles confined between two parallel plates. This $2D$ granular system allows mobility and cluster measurements by tracking the grain position/motion during successive taps. Our experimental results will relate the characteristics of the granular packing at various scales. Experimentally, the tracking of the grain motion is difficult inside a 3D granular pile. Therefore, we have performed simulations using the contact dynamics model. The preliminary results of these 3D simulations allow to discuss the difference between the two-dimensional and the three-dimensional cases.

2. Experimental study

2.1. Experimental set-up

Spherical metallic particles are placed between two parallel plates. The number of particles is typically $N \approx 2000$. The mean bead diameter is $D = 2.4$ mm, with a polydispersity smaller than 3.6%. The distance between both plates is slightly greater than the particle diameter. The width of the pile is 58 mm ($\approx 25D$) and the mean height is 170 mm ($\approx 70D$). A sketch and a picture of the setup are given in Figure 1. For producing the successive taps, an electro-mechanic hammer is placed below the container. The hammer is controlled by a micro-controller that can adjust the intensity, the number and the frequency of the taps.

The pile is illuminated with a single light source. In such a way, the center of each particle appears bright on the pictures taken by a high-resolution CCD camera. This camera can record an image of the packing after each tap. The position of each grain in the packing is later determined by image analysis. All grain positions are tracked by studying the correlations

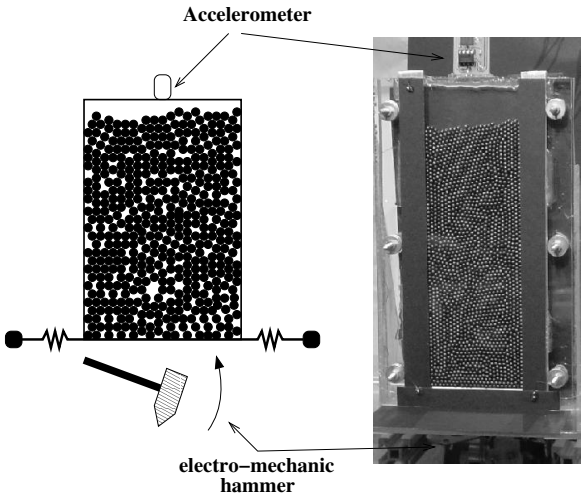

Figure 1. A sketch (left) and a picture (right) of our experimental setup. Approximately 2000 beads are placed between two parallel plates. An electro-mechanic hammer is placed below the pile and is controlled by a micro-controller. An accelerometer is placed on the vessel for measuring the acceleration experienced by the whole system.

between successive images [19]. The global packing fraction ρ of the pile is the ratio between the total area of the grains and the total area of the packing. Then, one has

$$\rho = \frac{N\pi D^2}{4S_{pile}} \tag{5}$$

where N is the number of grains in the pile and D is the grains diameter. The area of the pile S_{pile} is evaluated by determining the positions of the particles being placed on the top of the heap. Since the dynamics of the system slows down with the number of taps n, we recorded images of the system only for $n = 2^i$ with $i = 1, 2, ..., 16$. The maximum number of taps in our experiments is $n = 65536$.

2.2. Tap characteristics

We use an original system in order to produce taps. As we can see in Figure 2a, the system undergoes a short and strong peak of negative acceleration during a tap. The width of the main peak is 0.25 ms and the maximum intensity reaches -15g. Some damped oscillations during a few milliseconds are observed. The movement amplitude of the system is very small with respect to others. In both Rennes [8, 9] and Chicago [7, 13, 23] experiments, taps are produced by an electromagnetic exciter and consist of an entire cycle of a sine wave. For high accelerations, the considerable amplitude of the container produces some convection in the pile. It should be noted that such a global motion is not present in our experiment.

2.3. Compaction curves

We have repeated the experiment five times for statistical reasons. Obviously, small changes in the initial configurations of the packing give different values for ρ_0 and ρ_∞. Nevertheless, measurements of $\rho_0 = 0.825 \pm 0.002$ are reproducible. The last measurement $\rho(65536)$ of each series is assumed to be the asymptotic value $\rho_\infty = 0.862 \pm 0.004$. This value is slightly smaller than the hexagonal packing fraction $\rho_h \simeq 0.91$. This difference can be explained by the presence

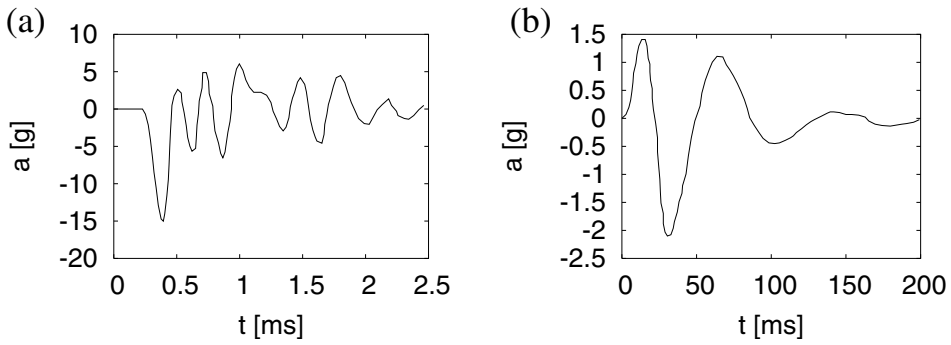

Figure 2. (a) Acceleration experienced by our system during a tap produced by an electromechanic hammer. The system undergoes a short peak of acceleration. The width of the main peak is 0.25 ms and the maximum intensity is 15 g. Some damped oscillations are observed during a few milliseconds. (b) Acceleration experienced by the system during a tap produced by an electromagnetic exciter in both Rennes [8, 9] and Chicago [7, 13, 23] experiments.

of defects due to edge effects, the presence of trapped defects and by the small polydispersity of the grains.

Since both initial ρ_0 and final ρ_∞ packing fractions depend on experimental conditions, a normalized parameter is defined. One has

$$\tilde{\rho} = \frac{\rho - \rho_0}{\rho_\infty - \rho_0}, \tag{6}$$

with $0 \leq \tilde{\rho} \leq 1$. The evolution of the normalized packing fraction $\tilde{\rho}$ as a function of the tap number n is presented in Figure 3. After 65536 taps, the saturation of the packing fraction is clearly obtained. The compaction curve is fitted by the logarithmic law Eq.(1) and the law Eq.(9) presented in the next section. Both laws fit correctly the compaction dynamics. However, oppositely to the logarithmic law, our law (9) fits the saturation of the density for large value of the tap number n.

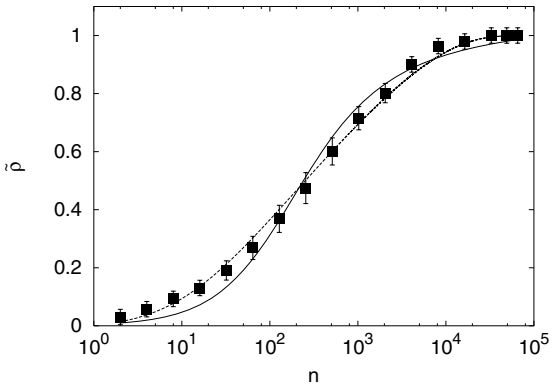

Figure 3. A typical curve giving the normalized packing fraction $\tilde{\rho}$ as a function of the tap number n. The solid curve is a fit using Eq. (1). The dashed curve is a fit using Eq. (9).

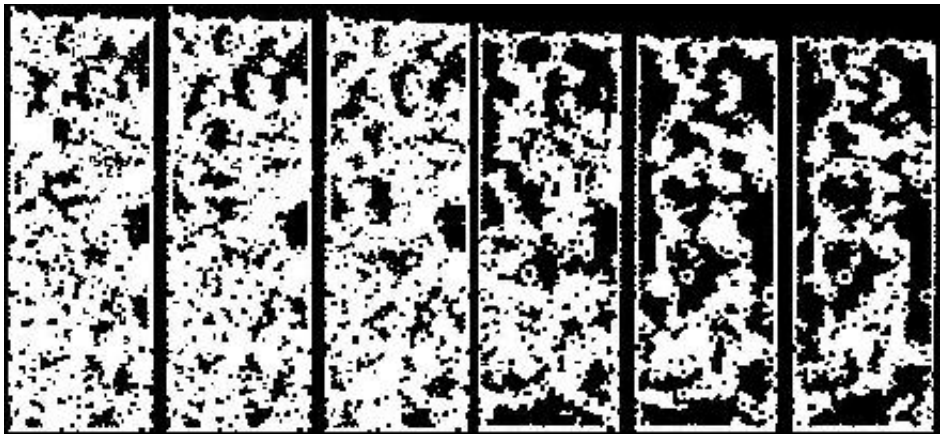

Figure 4. Pictures of the pile for $n = 0, 64, 128, 512, 4096, 65536$. Only grains belonging to hexagonal domains are colored. The growth and fusion of domains is clearly seen.

2.4. Grain organization

Our image analysis allows to determine the number of neighbors for each grain. Two grains are neighbors if their centers are separated by less than $D + \epsilon$ with $\epsilon \ll D$. The slight parameter ϵ is required because of the small polydispersity of the grains and because of the uncertainties on the grain positions. Typically, $\epsilon \approx D/15$. Grains belonging to hexagonal domains, i.e. being in contact with six neighbors, are shown in Figure 4. One should note that the grains located along the domain boundaries are not considered. As we can see on Figure 4, the pile is initially disordered: the average coordination number is low. After a few taps, small hexagonal domains appear and start to grow. At the end of the compaction process, some defects still remain and create domain boundaries in the system. We have measured the number of hexagonal domains and their mean area. The normalized fraction $\tilde{\phi}$ of grains belonging to hexagonal domains in the system has been determined.

Figure 5 presents the normalized fraction $\tilde{\phi}$ of hexagonal domains as a function of the number of taps n. This growth is well described by the theoretical Avrami model

$$\tilde{\phi} = 1 - \exp\left(-\left(\frac{n}{\tau}\right)^{\alpha}\right), \tag{7}$$

where τ is a characteristic time [28]. The Avrami model describes the crystallization kinetics of various coexisting growing domains. The value of the parameter α depends on the nature of the growth. The experimental data are well fitted by this equation with an exponent $\alpha = 0.42 \pm 0.09$. In the Avrami's theory, the value $\alpha = 1/2$ is a clear signature of a diffusion-controlled growth of hexagonal domains. This diffusive character could be understood as originating from the motion of defects along the borders of hexagonal domains. Indeed, the grains not belonging to hexagonal domains are supposed to have a higher mobility than others.

In order to relate this mesoscopic view of compaction to the macroscopic measurements, we have drawn in Figure 6 the fraction $\tilde{\rho}$ as a function of the fraction $\tilde{\phi}$. We have

$$\tilde{\rho} = \sqrt{\tilde{\phi}}, \tag{8}$$

which is illustrated by the continuous curve on the Figure 6. This square root behaviour means that the defects (leading to a lower density) are only located along the perimeter of the clusters.

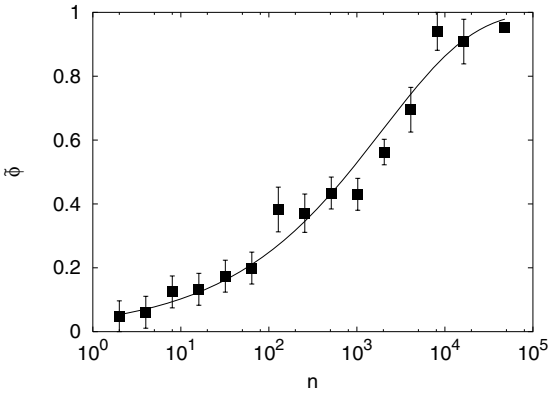

Figure 5. Evolution of the normalized fraction $\tilde{\phi}$ of hexagonal domains as a function of the tap number n. The continuous curve is a fit using Eq.(7).

This relationship allows us to propose a new law for compaction dynamics

$$\tilde{\rho} = \sqrt{1 - \exp\left(-\sqrt{\frac{n}{\tau}}\right)}, \tag{9}$$

which is an alternative to the inverse logarithmic law (1) in $2D$. This law could be adjusted to experimental data as seen in Figure 3. The agreement is excellent. Furthermore, this law has the advantage to present a clear saturation for large n values, a saturation which was not accurately fitted by the law (1). The validity of this law has been checked with other tap intensities. If we assume that the normalized packing fraction $\tilde{\rho}$ increases linearly with the fraction of hexagonal domains $\tilde{\phi}$ (this assumption becomes reasonable when $0.3 < \tilde{\rho} < 1$), we recover the KWW law [9] for the evolution of $\tilde{\rho}$.

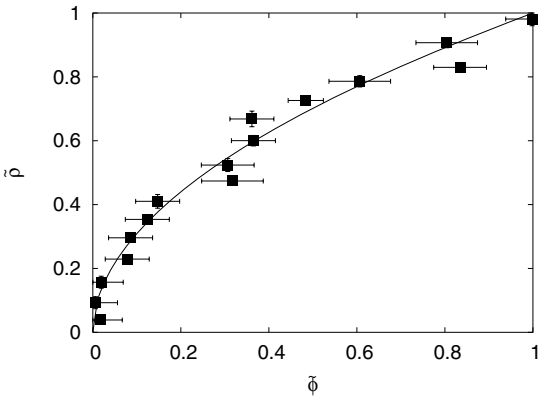

Figure 6. Evolution of the normalized packing fraction $\tilde{\rho}$ according to the normalized hexagonal domains fraction $\tilde{\phi}$.

2.5. Grain mobilities

Since all the grain positions (x_i, y_i) are determined, it is possible to measure the displacement δ_i of the grain i during a tap. One has

$$\delta_i = \frac{\sqrt{\delta x_i^2 + \delta y_i^2}}{\Delta n}, \tag{10}$$

where Δn is the number of taps realized between two successive pictures. A dimensionless average mobility μ can be defined from the ratio between particle displacements δ_i and particle diameters D. One has

$$\mu = \frac{1}{N} \sum_{i=1}^{N} \frac{\delta_i}{D}, \tag{11}$$

which can be easily computed. Figure 7 shows the decrease of the mobility μ according to the normalized packing fraction $\tilde{\rho}$. The non-zero value of the mobility for $\tilde{\rho} = 1$ is due to the finite spatial resolution of the camera and uncertainties on grain positions. These experimental results can be fitted by the Vogel-Fulcher law Eq.(3) with $\mu_0 = 0.015 \pm 0.008$ and $c = 2.1 \pm 0.3$. The agreement is good for high values of the normalized packing fraction ($\tilde{\rho} > 0.3$). Injecting the Volger-Fulcher law in the equation (2) leads to a solution [14] that corresponds to the inverse logarithmic law (1). The latter law correctly fits the data of Figure 3, except at the end of the process when a saturation is observed. Injecting the Avrami law (9) in the equation Eq.(3) gives an expression for the mobility evolution. One has

$$\mu = -\frac{1}{k} \frac{1 - \tilde{\rho}^2}{\tilde{\rho}\ \ln(1 - \tilde{\rho}^2)}. \tag{12}$$

The experimental results are well fitted by this law in Figure 7.

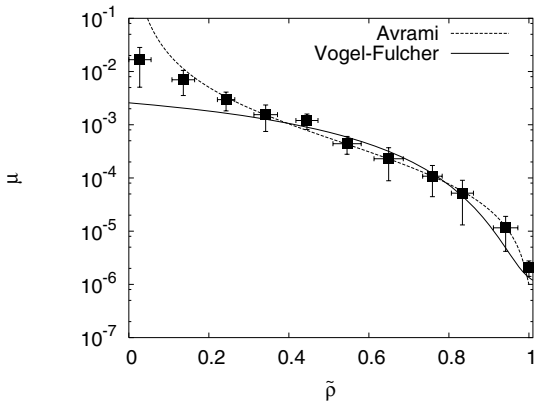

Figure 7. Grain mobility μ as a function of the normalized packing fraction $\tilde{\rho}$. These results come from an average over various experiments. Error bars are indicated. The continuous curve is a fit of the Volger-Fulcher law (Eq 3). The dashed curve is a fit with the Avrami law (Eq 12).

3. Simulations

3.1. The contact dynamics model

Different approaches exist to simulate the slow dynamics of granular media. The oldest and the most used is the lattice model [11, 12, 5] that find many applications. Recently, new numerical

models based on force calculation have been developed in order to compute the velocity of each grain composing the granular system [30]. This family of models is called DEM (Discreet Element Method). Lattice models are faster than DEM models but are limited for the study of macroscopic physical parameters. They reproduce the behavior of the density, for example. In opposition, DEM allows to change some microscopic parameters that characterize the grains and the container walls or give access to many informations like the force network.

Two kinds of DEM exist: the molecular dynamics and the contact dynamics. The main difference between both models is the evaluation of the contact forces. For the molecular dynamics models, the normal force is calculated by the interpenetration of antagonist and protagonist grains. On the contrary, the contact dynamics follows a theoretical method called "No Smooth Contact Dynamics" (NSCD) [31], where the normal contact force is estimated by the Signorini diagram (see Fig. 8).

The major consequence of contact force evaluation is the physical time scale associated to the numerical iterations. In molecular dynamics, the numerical time step is limited by the physical time scale associated to the collisions of grains. As a consequence, the numerical time step is roughly equals to 10^{-6} second. On the other hand, the contact dynamics considers that the physical time scale of contact is zero. Therefore, the time step is linked to the displacement time of the grains. The different scales for DEM induce different applications. The molecular dynamics is more adapted to the study of granular flows and the contact dynamics is better suited to static and quasi static studies like granular compaction.

The contact dynamics is often applied in two-dimensional problems. In the last few years, a three-dimensional version of this model was implemented. In the case of granular compaction, numerical studies have been realized with purely geometrical model like Tetris model [11] in two dimensions and models of P. Philippe *et al.* in three dimensions [9]. Our study of granular compaction is the first one in three dimensions based on contact dynamics.

The contact dynamics computes the velocity of each solid that composes the system for the six degrees of freedom in the case of a three-dimensional problem. This model is based on the NSCD using the two diagrams of Signorini and Coulomb (Fig. 8) for the normal (N) and the tangential (T) contact forces respectively versus the relative normal (v_n) and tangential (v_t) velocity between the grains in a local contact base. Some physical hypotheses are considered.

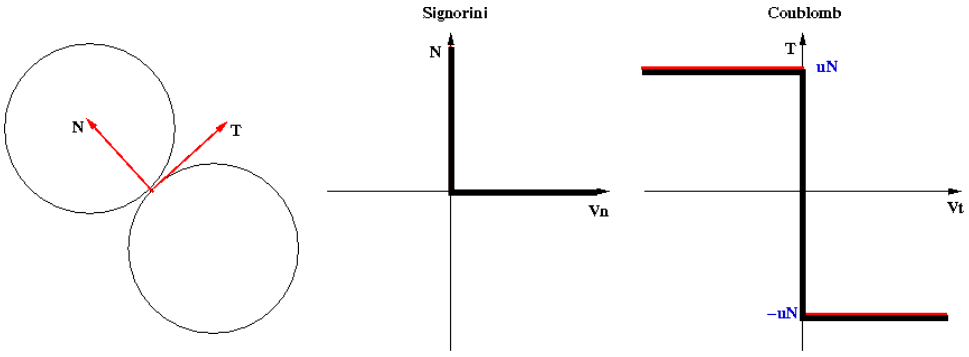

Figure 8. (left) Normal (N) and tangential (T) forces in a contact between two spherical grains. (right) Signorini and Coulomb diagrams used in NSCD.

First, no force depends on the interpenetration at the contact, in opposition to the molecular dynamics. The normal relative velocity is thus equals or higher than zero as presented in the Signorini diagram (center, Fig. 8). The normal contact force is not zero only when the relative normal velocity is zero. The tangential contact force is equals to $\pm\mu N$ when the relative

tangential velocity is strictly under or over zero respectively; when the relative tangential velocity is zero the tangential contact force is between the values $\pm\mu$N as presented in the Coulomb diagram (Fig. 8, right).

The first step of the model consists in creating a pile of spheres that has a low volume density. Different methods are commonly encountered to realize compaction experiments: for example, in Chicago, a gas is injected at the bottom of the container; at the GMCM in Rennes, a grid is displaced upwards through the granular piling. The experimental methods present many difficulties for implementation in our numerical model. Thus, we must create an artificial method to build a low density pile. This one uses extreme values for the friction and restitution coefficients during the initialisation of the pile. The initialisation consists on placing the grains on a three-dimensional lattice with a two-dimensional white noise around the cubic lattice. Then the relaxation driven by the gravity. After pile formation, the physical values of the coefficients are corrected before starting the process of compaction. The advantage of this method is that simulated piles have the same initial density than the experimental ones (≈ 0.57).

3.2. Tap characteristics

Numerically, a strong and short peak of acceleration is hard to simulate. Therefore, in our model, we reproduce the experimental taps from both Rennes and Chicago (see Figure 2b). We reproduce easily this kind of tap by imposing the velocity to the container along the vertical direction. The dimensionless intensity parameter Γ is defined by

$$\Gamma = \frac{A\omega^2}{g}, \tag{13}$$

where A is the amplitude of the oscillations, ω is the angular velocity and g is the gravitational acceleration. Between two consecutive taps, the relaxation process must be last long enough to allow every grain in the pile to reach a stable position. Our relaxation time corresponds to the experimental measurements from Rennes.

3.3. Compaction curve

The model reproduces realistic compaction curves from an initial density value $\rho_0 = 0.57$ and for various intensities Γ of the taps (see Fig. 9). The curves are fitted by a stretched exponential law (4). The final values of the density obtained after 100 taps increased with the tap intensity Γ. Moreover, the characteristic time τ decrease with tap intensity Γ as observed in the experiments.

3.4. Grain organization

During the first 100 taps and for tap intensities Γ situated between 2 and 10, we do not observe any global crystallization. Oppositely to our 2D experiment, the system remains amorphous.

3.5. Mobility

By tracking each grain during the process of compaction, the mobility μ is measured. The figure 10 displays the average grain mobility μ (the average displacement of a grain during one tap) as a function of the normalized density $\tilde{\rho}$ for different tap intensities Γ. Curves are similar to experimental data (see Figure 7) except that a residual mobility is still present in simulations. The mobility is higher when the intensity is higher.

4. Conclusion

We have measured three physical quantities during the compaction of 2D isotropic granular materials. They correspond to three different scales in the system. First, we have confirmed that the logarithmic law (1) for the density evolution and the Vogel-Fulcher law (3) for the

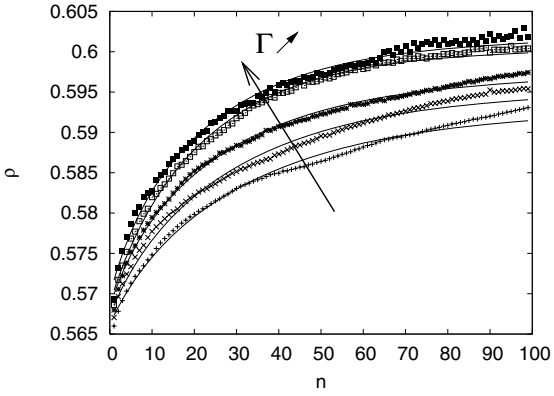

Figure 9. Evolution of the density ρ of a packing composed by 4114 spheres submitted to a series of identical taps. Different taps intensities are illustrated from $\Gamma = 2$ to $\Gamma = 10$.

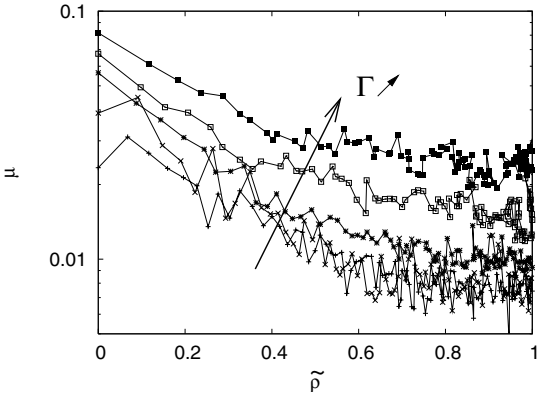

Figure 10. Evolution of the grain mobility μ of a packing composed of 4114 spheres as a function of ρ. Different taps intensities are illustrated from $\Gamma = 2$ to $\Gamma = 10$.

mobility decreases are good candidates for describing the compaction dynamics of a 2D pile of spherical particles. Moreover, we have shown that granular compaction dynamics in 2D could be viewed as a slow process of crystallization driven by the diffusion of defects. The resulting laws (7), (9) and (12) are consistent with experimental data. The 3D simulations with the contact dynamics reproduces the compaction dynamics and the behavior of the grain mobility. The preliminary results of these simulations show that the major difference between the 2D and the 3D case is the absence of crystallisation in 3D.

5. Outlook

The contact dynamics model is a very good tool to investigate the granular compaction. Indeed, within this model, we have obtained to the contact and force network inside the pile. The analysis of these networks evolution during the compaction process could explain phenomena like ageing and memory effects. We can also vary easily physical quantities like restitution and frictional coefficients.

In the real life, granular materials are rarely composed of perfectly spherical particles. Recently, some studies on anisotropic granular materials have been performed [20, 21, 22, 23, 24,

25, 26]. The major difference between spherical grains and anisotropic grains is the tendency of anisotropic grains to align themselves along their symmetry axis. The anisotropic grains have also the tendency to align themselves along the container walls [21]. Therefore, during the compaction process, the grain orientations become an important parameter.

Actually, our experimental studies of compaction are focused on anisotropic granular materials. At the microscopic scale, we measure both translational and rotational mobilities. Therefore, we can determine the effect of the grain rotations on the compaction process. At the mesoscopic scale, we observe the formation and the growth of domains made of aligned grains. For more details, see the preprint [29].

6. Acknowledgements

This work has been supported by the contract ARC 02/07-293. FL benefits of a FRIA (Brussels, Belgium) grant. The authors thank the organizers and the lecturers of the sommerschule AGEING AND THE GLASS TRANSITION 2005. We gracefully acknowledge useful discussions with C. Becco, H. Caps, E. Clément, S. Dorbolo and P. Richard for valuable discussions.

References

[1] P. G. de Gennes, Rev. Mod. Phys. **71**, S374 (1999)
[2] H. M. Jaeger, S. R. Nagel and R. P. Behringer, Rev. Mod. Phys., **68**, 1259 (1996)
[3] J. Duran 1999, *Sables, poudres et grains* (Paris: Eyrolles Sciences)
[4] A. Kudrolli, Rep. Prog. Phys. **67**, 209 (2004)
[5] F. Ludewig and N. Vandewalle, Euro. Phys. J. E **18**, 367 (2005)
[6] E. R. Nowak, J. B. Knight, E. Ben-Naim, H. M. Jaeger, and S. R. Nagel, Phys. Rev. E **57**, 1971 (1998)
[7] J. B. Knight, C. G. Fandrich, Chun Ning Lau, H. M. Jaeger, and S. R. Nagel, Phys. Rev. E **51**, 3957 (1995)
[8] P. Richard, M. Nicodemi, R. Delannay, P. Ribière, and D. Bideau, Nature Materials **4**, 121 (2005)
[9] P. Philippe, and D. Bidau, Europhys. Lett. **60**, 677 (2002)
[10] G. Lumay and N. Vandewalle, Phys. Rev. Lett. **95**, 028002 (2005)
[11] E. Caglioti, V. Loreto, H.J. Herrmann and M. Nicodemi, Phys. Rev. Lett. **79**, 1575 (1997)
[12] F. Ludewig, S. Dorbolo and N. Vandewalle, Phys. Rev. E **70**, 051304 (2004)
[13] E. Ben-Naim, J. B. Knight, E. R. Nowak, H. M. Jaeger, and S. R. Nagel, Physica D **123**, 380 (1998)
[14] T. Boutreux and P.G. de Gennes, Physica A **244**, 59 (1997)
[15] Y. Levin, J.J. Arenzon and M. Sellitto, Europhys. Lett. **55**, 767 (2001)
[16] J.J. Arenzon, Y. Levin and M. Sellitto, Physica A **325**, 371 (2003)
[17] P.N. Pusey and W. van Megen, Nature **320**, 340 (1986)
[18] K. L. Gavrilov, Phys. Rev. E **58**, 2107 (1998).
[19] The tracking of the grain is based on an algorithm developped in our group. This technique has already been used in various works : N.Vandewalle, S.Trabelsi and H.Caps, Europhys. Lett. **65**, 316 (2004) ; H.Caps, S.Trabelsi, S.Dorbolo and N.Vandewalle, Physica A **344**, 424 (2004).
[20] D.L. Blair, T. Neicu, and A. Kudrolli, Phys. Rev. E **67**, 031303 (2003)
[21] G. Lumay and N. Vandewalle, Phys. Rev. E **70**, 51314 (2004)
[22] P. Ribière, P. Richard, R. Delannay and D. Bideau, Phys. Rev. E **71**, 011304 (2005)
[23] F. X. Villarruel, B. E. Lauderdale, D. M. Mueth, and H. M. Jaeger, Phys. Rev. E **61**, 6914 (2000)
[24] K. Stokely, A. Diacou, and Scott V. Franklin, Phys. Rev. E **67**, 051302 (2003)
[25] A.P. Philipse and A. Verberkmoes, Physica A **235**, 186 (1997)
[26] S.R. Williams and A.P. Philipse, Phys. Rev. E **67**, 051301 (2003)
[27] P. Philippe, *Etude théorique et expérimentale de la densification des milieux granulaires*, PhD thesis, Université de Rennes 1, (2002)
[28] M. Avrami, J. Chem. Phys. **7**, 1103-1112 (1939); M. Avrami, J. Chem. Phys. **8**, 212 (1940)
[29] G. Lumay and N. Vandewalle, cond-mat/0510242 (2005)
[30] M. Renouf and P. Alart, Comp. Meth. Appl. Mech. Eng., vol. **194/18-20**, 2019 (2004)
[31] J. J. Moreau, Revue Européenne des Eléments Finis **10**, 1 (2000)